# Crystallographic mapping and tuning of water adsorption in metal-organic frameworks featuring distinct open metal sites

Yi Han\*,# Prasenjit Das#, Yiwen He, Dan C. Sorescu, Kenneth D. Jordan, and Nathaniel L. Rosi\*

**ABSTRACT:** Crucial steps toward designing water sorption materials and fine-tuning their properties for specific applications include precise identification of adsorption sites and establishment of rigorous molecular-level insight into the water adsorption process. We report stepwise crystallographic mapping and DFT computations of adsorbed water molecules in ALP-MOF-1, a metal-organic framework decorated with distinct open metal sites and carbonyl functional groups that serve as water anchoring sites for seeding the nucleation of a complex water network. Identification of an unusual water adsorption step in ALP-MOF-1 motivated the tuning of metal ion composition to carefully adjust water uptake. These studies provide direct evidence that the identity of the open metal sites in MOFs can dramatically affect water adsorption behavior between 0 and  $\sim 20\%$  RH and that multiple proximal water anchoring sites along the MOF skeleton facilitate water uptake steps which could be potentially useful for applications requiring rapid and energetically facile water sorption.

#### INTRODUCTION

Porous metal-organic frameworks (MOFs)1,2 have been extensively explored as sorbents for a range of small molecules.<sup>3-6</sup> A growing number of reports have examined water adsorption in MOFs7 and evaluated them as candidate materials for water harvesting,8-11 dehydration12, and adsorptive moisture control13 or refridgeration.14 Each of these applications requires specific water sorption properties which in principle could be adjusted by fine-tuning adsorption sites at the atomic level to control sorbent-sorbate interactions. Diffraction studies have proven useful for identifying small molecule adsorption sites in MOFs and for tracking processes in situ, leading to rational design aimed at tailoring structure and properties. 15-23 Tracking water adsorption in MOFs at different loadings in a step-by-step fashion would permit unambiguous identification of adsorption sites and a thorough understanding of chemical and structural factors that affect the sorption profile.24-28 Indeed, a recent single-crystal X-ray diffraction (SCXRD) study elucidated the effect of ligand functionality on the water sorption properties of MOF-303 and -333.29 While tuning ligand chemistry is one way to adjust small molecule adsorption in MOFs, it is well-known that metal ions are often the strongest adsorption sites, and their relative Lewis acidity can impact small molecule adsorption properties most dramatically.30

Here, we present crystallographic snapshots of adsorbed water molecules in porous MOF crystals with distinct open metal sites. Combining experiments and electronic structure calculations, we i) monitor water adsorption from zero loading through pore filling, ii) reveal and describe the origin of an unusual water uptake phenomenon, and iii) identify how metal ion identity affects the water uptake properties. Insights gained from these studies serve as the basis for modulation of the metal ion composition to carefully tune water adsorption in the 0-20% range of relative

humidity (RH), relevant to potential applications ranging from water harvesting to dehydration.<sup>7</sup>

#### RESULTS AND DISCUSSION

MOF Preparation and Characterization. We have a longstanding interest in the structure and chemistry of MOFs constructed from mixtures of multicarboxylate linkers and N-heterocyclic bases (e.g., purines and related bases). 31-33 This study began with the identification of ALP-MOF-1, a zinc-terephthalate-allopurinol MOF. Heating a mixture of Zn(NO<sub>3</sub>)<sub>2</sub>·6H<sub>2</sub>O, allopurinol (H<sub>2</sub>ALP), and terephthalic acid (H<sub>2</sub>BDC) in dimethylacetamide (DMA) and H<sub>2</sub>O vielded colorless single crystals of ALP-MOF-1-AS (AS = as-synthesized), formulated as  $[Zn_2(\mu_2-H_2O)(ALP)(BDC)]\cdot 2DMA,H_2O$ . SCXRD studies revealed an extended 3-D porous structure (Figure 1a) consisting of interconnected  $Zn_4(\mu_2$ -H<sub>2</sub>O)<sub>2</sub>(ALP)<sub>2</sub>(BDC)<sub>2</sub> clusters (Figure 1b). Two equivalent edge-sharing Zn(II) octahedra bridged by two  $\mu_2$ -H<sub>2</sub>O and two ALP sit at the center of each cluster. They are flanked by two additional equivalent Zn(II) tetrahedra which connect to the octahedral Zn(II) through the carboxylates of two BDC and the N-N linkage in ALP. The clusters serve as 8-connected vertices, and the MOF adopts the ecz network topology (Figure S1).

One guest water molecule in addition to two DMA molecules were resolved in the crystal structure of ALP-MOF-1- AS (Figure S2a): the DMA guests form hydrogen bonds with the  $\mu_2$ -H<sub>2</sub>O and the guest water forms a hydrogen bond with the carbonyl O of ALP. Solvent exchange studies were performed to assess guest molecule mobility. Thorough washing with acetone yielded ALP-MOF-1-acetone, in which the two DMA molecules were replaced with one acetone and one water molecule, each hydrogen bonded to the  $\mu_2$ -H<sub>2</sub>O; the other guest water molecule remained in a similar bonding environment, hydrogen bonded to the ALP carbonyl O (Figure S2b). These observations indicate that the  $\mu_2$ -H<sub>2</sub>O

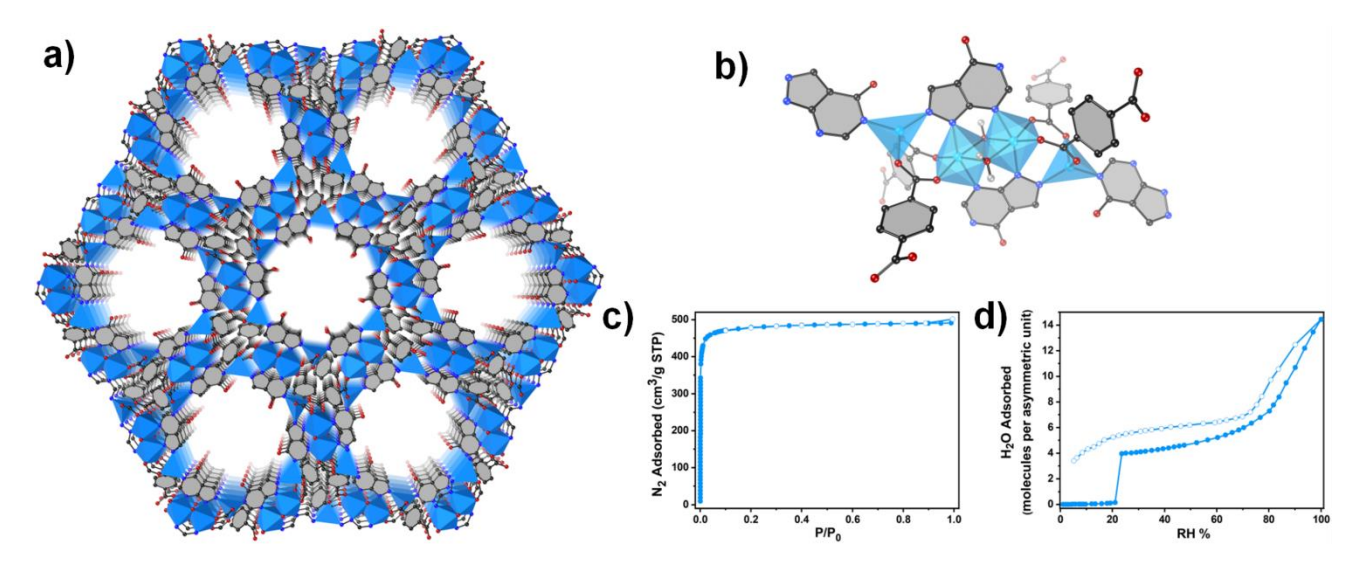


**Figure 1.** Single crystal structure and  $N_2$ /water sorption of ALP-MOF-1. a) The crystal structure of ALP-MOF-1-*AS* has channels that run along the *c* crystallographic axis which are lined with the C=O groups of ALP (note: guest solvent molecules omitted for clarity). b) The Zn(II) clusters within ALP-MOF-1-*AS* contain two edge-sharing Zn(II) octahedra bridged by two ALP and two  $\mu_2$ -H<sub>2</sub>O. The octahedral Zn(II) are bridged to peripheral tetrahedral Zn(II) through the N-N linkage on ALP as well as carboxylates of 4 BDC ligands (Zn, light blue polyhedra; C, black spheres; O, red spheres, N, dark blue spheres; H, light gray spheres, omitted for clarity in framework depiction shown in part a). In total, each cluster has 8 ligands which link to neighboring clusters to form the extended 8-connected framework. c) The N<sub>2</sub> sorption isotherm (77 K) of ALP-MOF-1-*A*. d) The water sorption isotherm collected at 298 K for ALP-MOF-1-*A* shows an abrupt uptake of four water molecules per asymmetric unit at ~23% RH followed by a gradual uptake to note filling at ~100% RH (adsorption: filled circles: desorption: empty circles)

and the proximal ALP carbonyl O are hydrogen bonding anchoring sites, and that ALP-MOF-1 could potentially serve as a scaffold for adsorbing water. Moreover, these findings also point toward the potential of tracking water adsorption in ALP-MOF-1 and mapping the water network within the pores with the aim of identifying chemical and structural features that impact water sorption. Ultimately, those features might be considered 'design attributes' for incorporation into future target MOFs.

We first explored activation conditions to evaluate the permanent porosity of ALP-MOF-1. Thermal gravimetric analysis (TGA) of ALP-MOF-1-acetone indicated complete removal of all solvent, including water, upon heating to ~75 <sup>o</sup>C (Figure S3b). Activation of ALP-MOF-1-acetone was achieved via evacuation at room temperature for 24 h, which yielded ALP-MOF-1-A (A = activated), formulated as Zn<sub>2</sub>(ALP)(BDC). The compositions of all ALP-MOFs reported herein were determined through a combination of elemental analysis (EA), proton nuclear magnetic resonance (1H NMR) spectroscopy (Figure S4), and TGA (Figure S3 and S14b). SCXRD data for ALP-MOF-1-A were collected and confirmed solvent removal, including the coordinated water bridging the two central Zn(II) within the clusters (Figure 2a and S2c). The observation that the coordinated water could be removed either by heating at temperatures under 100 °C or simply under vacuum suggested rather weak association with the Zn(II) sites. Indeed, the Zn-O bond lengths in ALP-MOF-1-acetone for the asymmetrically coordinated water molecules are 2.244 Å and 2.406 Å, which are greater than typical Zn-O bond lengths ( $\sim$ 2.027 Å) in Zn-aqua complexes.34 This weakly coordinated water may be held in position to some extent through hydrogen bonding with neighboring solvent: the 0...0 distance between the acetone and the coordinated water is 2.760 Å,

which falls within the sum of the van der Waal radii and is typical for water-water hydrogen bonding. Thus, removal of guest solvent (e.g., acetone) may then destabilize the coordinated water and facilitate its removal under relatively mild activation conditions.  $N_2$  adsorption (77 K) experiments were conducted on ALP-MOF-1-A. It exhibits a Type I isotherm characteristic of a microporous material and has a Brunauer-Emmett-Teller (BET) surface area of  $\sim 1900 \text{ m}^2/\text{g}$  (Figure 1c). The pore size distribution reveals two pores centered at  $\sim 9.5$  and 12 Å (Figure S5), which corresponds well with the crystal structure (Figure S6).

Water Sorption Properties of ALP-MOF-1. Having established conditions for removing all solvent and water and achieving permanent microporosity, we next collected the room temperature water vapor isotherm (Figure 1d). ALP-MOF-1-A shows negligible adsorption until ~23% RH, at which point the water uptake abruptly increases to  $\sim$ 16.8 wt% ( $\sim$ 210 cc/g), which is equivalent to  $\sim$ 4 H<sub>2</sub>0 per asymmetric unit (Zn<sub>2</sub>(ALP)(BDC)), Between 23% and 100% RH. the water loading gradually increases to ~60.6 wt% (~760 cc/g), ~14.4 H<sub>2</sub>O per asymmetric unit. Hysteresis is observed upon desorption under vacuum; at the end of the water sorption experiment ~3.3 water molecules per asymmetric unit remain in the MOF. The water sorption experiment apparently compromises the MOF structure, as evidenced by disappearance of the diffraction peak at  $\sim 5^{\circ}$  20 corresponding to the (2,-1,0) plane and broadening and shifting of other higher angle peaks (Figure S7a). Further, a second subsequent water adsorption experiment on the same sample showed a significant decrease in water uptake (Figure S8). We note that ALP-MOF-1-AS remains highly crystalline after soaking in water for 12h (Figure S7a), yet its N<sub>2</sub> uptake at 77 K decreases slightly (Figure S7b). Nevertheless, these features do not preclude the use of ALP-MOF-

1 as an important model system for examining and understanding the effects of MOF composition and structure on water uptake phenomena.

 $\sim\!100\%$  RH (complete pore filling). Fourier-transform infrared (FTIR) spectroscopy was used to gain insight into the interactions between the framework and adsorbed water

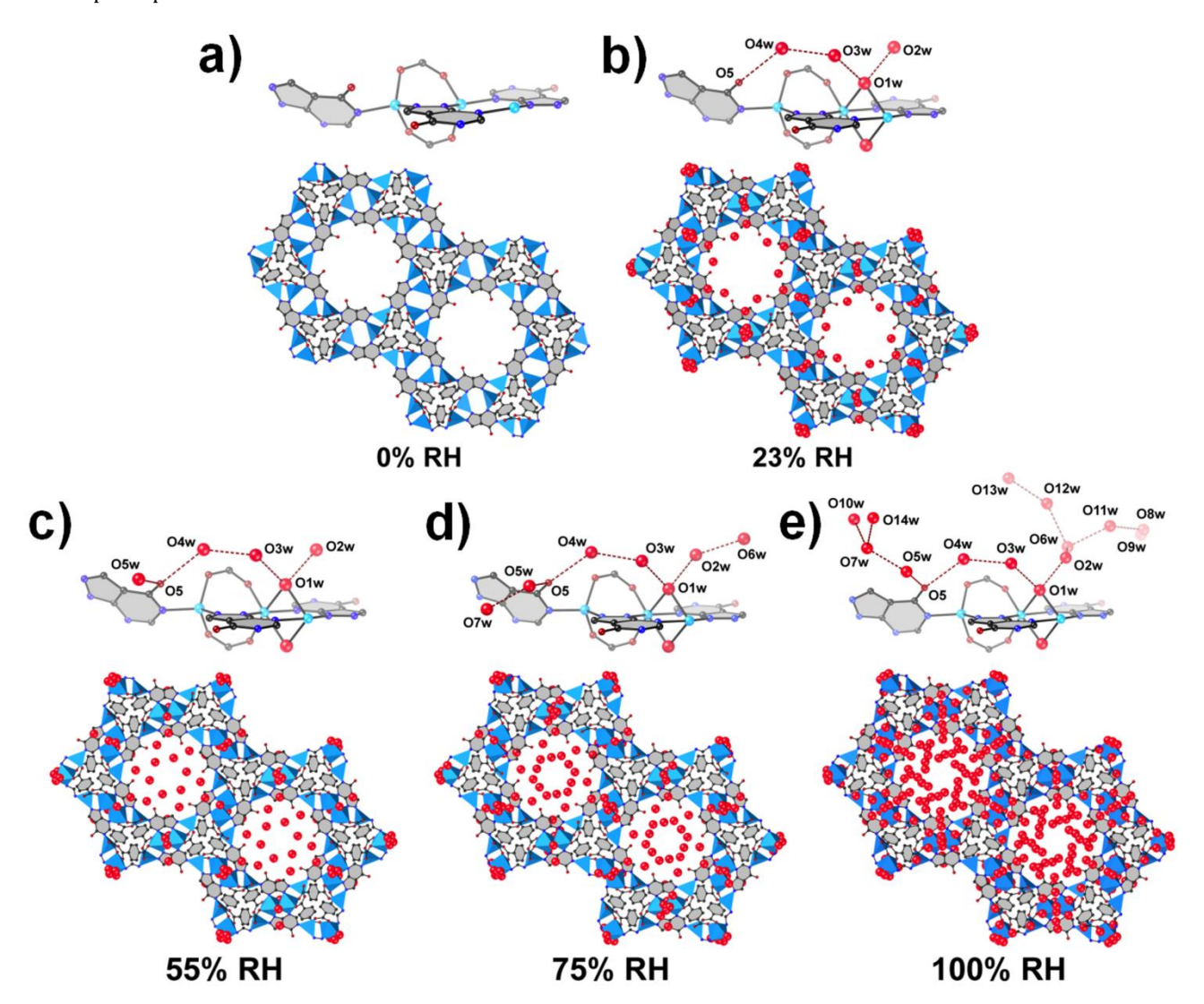


**Figure 2.** Crystallographic snapshots of water molecule loading in ALP-MOF-1-*A*. a-e) Two depictions of the structures: top, fragment around Zn(II) cluster; bottom, view of channel along *c* crystallographic direction (Zn, light blue spheres and polyhedra; C, black spheres; N, dark blue spheres; framework O, small dark red spheres; water O; large bright red spheres; H omitted for clarity). a) ALP-MOF-1-*A*, with all solvent and water removed, including bridging  $\mu_2$ -H<sub>2</sub>O. b) ALP-MOF-1-*4H*<sub>2</sub>O formed after exposure to ~23% RH (4 water molecules per asymmetric unit, 01w-04w) (Zn-01w = 2.262 and 2.396 Å; 01w···02w = 2.683 Å; 01w···03w = 2.698 Å; 03w···04w = 2.845 Å; 05···04w = 3.037 Å). c) ALP-MOF-1-*5H*<sub>2</sub>O formed after exposure to ~55% RH (5 water molecules per asymmetric unit, 01w-05w) (Zn-01w = 2.253 and 2.388 Å; 01w···02w = 2.719 Å; 01w···03w = 2.712 Å; 03w···04w = 2.823 Å; 05···04w = 3.050 Å; 05···05w = 2.747 Å). d) ALP-MOF-1-*7H*<sub>2</sub>O formed after exposure to ~75% RH (7 water molecules per asymmetric unit, 01w-07w) (Zn-01w = 2.220 and 2.321 Å; 01w···02w = 2.680 Å; 01w···03w = 2.680 Å; 03w···04w = 2.884 Å; 05···04w = 3.033 Å; 05···05w = 2.600 Å; 05w···07w = 2.758 Å; 02w···06w = 2.813 Å). e) ALP-MOF-1-*14H*<sub>2</sub>O formed after exposure to ~100% RH (14 water molecules per asymmetric unit, 01w-014w) (Zn-01w = 2.200 and 2.282 Å; 01w···02w = 2.674 Å; 01w···03w = 2.692 Å; 03w···04w = 2.837 Å; 05···04w = 2.912 Å; 05···05w = 2.544 Å; 05w···07w = 2.691 Å; 02w···04w = 2.791 Å; 07w···010w = 2.741 Å; 07w···014w = 2.530 Å; 06w···011w = 2.826 Å; 06w···012w = 2.904 Å; 012w···013w = 2.769 Å; 011w···08w = 2.516 Å; 08w···09w = 2.870 Å). In b)-e). dashed lines between O atoms indicate hydrogen bonding interactions.

To probe water adsorption at the molecular level, we exposed individual samples of ALP-MOF-1-A to different levels of relative humidity, tracking the progression of the water adsorption isotherm. Four hydrated samples were selected:  $\sim\!23\%$  RH (the initial adsorption step);  $\sim\!55\%$  RH ( $\sim\!$ halfway along the isotherm);  $\sim\!75\%$  RH ( $\sim\!$ inflection point before steep rise in uptake signifying pore filling); and

(Figure S9a). With increasing RH, we observed a gradual increase in the broad water OH stretching band from 3600-3100 cm<sup>-1</sup> and a significant dampening and shift of the ALP carbonyl stretch observed at ~1700 cm<sup>-1</sup> in ALP-MOF-1-A. We attribute the latter observation to hydrogen bonding between adsorbed water and the ALP carbonyl. After exposure to these different RH levels, visual inspection under a

light microscope confirmed that the crystals remain transparent and maintain their shape. Indeed, for each hydrated sample, the framework remains crystalline (Figure S9). After exposure to ~23% RH, 4 crystallographically unique water molecules are located and we designate this material ALP-MOF-1-4H2O. The first water molecule, denoted by O1w (w for water) in Figure 2b (O6 in ALP-MOF-1- $4H_2O$ .cif), is the  $\mu_2$ -H<sub>2</sub>O bridging the two central Zn(II). Three additional areas of high residual electron density were assigned 02w-04w (07-09 in ALP-M0F-1-4H<sub>2</sub>O.cif). 02w and 03w are within hydrogen bonding distance of 01w while 04w links 03w and 05 (05 is the framework carbonyl oxygen). Thus, at ~23% RH, a hydrogen bonded chain of four water molecules ( $W_4$ ; W = water) forms along the framework backbone, while the middle of the pores remain empty (Figure 2b). Adsorption of these four water molecules occurs according to the first dramatic step in the water isotherm at ~23% RH. This unique water adsorption step highlights the structural importance of the carbonyl oxygen, in particular its proximity to the central Zn(II) dimer and its role as an 'anchoring' site for hydrogen bonding between the framework and the water chain.

Additional support for the configuration and formation of the water chains observed at ~23% RH was provided by density functional theory (DFT) calculations,36 using the dispersion-corrected PBE-D3 exchange correlation functional37,38 in connection with 3D periodic models based on the periodic unit cell of ALP-MOF-1-4H<sub>2</sub>O (Supplementary Section 3). We have further refined the structure by assigning the missing hydrogen atoms of different water molecules and fully optimizing both the adsorbed water molecules as well as the framework. In these calculations different orientations of water OH groups were considered. Our initial optimizations did not use crystal symmetry but refinements for the most stable configurations using symmetry gave essentially the same results. The results for the most stable configuration of the W<sub>4</sub> chain identified in the calculations corresponding to ~23% RH (Figure S20) reveal that O4w provides stabilization on one side of the W3 chain formed around the Zn-Zn bonding sites by hydrogen bonding to framework carboxyl groups. We next calculated average adsorption energies of the adsorbed water molecules and examined the binding of 01w both within the W4 chains and in isolation as a single molecule to gain some insight into the observed four water molecule adsorption step. The average adsorption energy of water molecules in the 18 W<sub>4</sub> chains formed in the entire MOF unit cell is 13.3 kcal/mol. This is larger than the 11.0 kcal/mol adsorption energy calculated for a single water molecule adsorbed between a pair of Zn(II) sites (Figure S21b). Notably, for the case of a single adsorbed water molecule, the DFT calculations predict that it is asymmetrically bonded to a pair of adjacent Zn(II) sites with average Zn···Ow separations of 2.44 and 3.24 Å; further, it adopts a tilted structure as a result of forming a hydrogen bond with a carboxyl O. When this water molecule is part of the more highly hydrated species involving the W<sub>4</sub> chains, it adopts a more symmetrical structure with shorter average Zn···Ow separations of 2.22 and 2.40 Å, which are comparable to the Zn···Ow separations observed in ALP-MOF-1-acetone. The water-water hydrogen bonding increases the polarity of the water molecules, which, in turn, results in stronger bonding to the Zn(II) ions, consistent with the reduction in the Zn···Ow distances. Thus, our DFT calculations indicate that 01w is significantly stabilized when it is within the W<sub>4</sub> chain, which helps explain why four water molecules adsorb at  $\sim\!23\%$  RH. It is also relevant to indicate that in the case of the W<sub>4</sub> chains, each pair of Zn(II) sites is involved in bonding with a second W<sub>4</sub> chain located below the Zn…ALP…Zn plane (Figure S20b). Moreover, the framework and the 18 W<sub>4</sub> chains identified at  $\sim\!23\%$  RH satisfy the R-3 hexagonal space group symmetry.

At ~55% RH, an area of diffuse electron density appears near 05, which we assign to another hydrogen bonded water molecule, 05w (010 in ALP-MOF-1-5H<sub>2</sub>O.cif; Figure 2c), resulting in formation of ALP-MOF-1-5*H*<sub>2</sub>*O*; two additional waters, 06w and 07w, (011 and 012 in ALP-M0F-1- $7H_2O$ .cif; Figure 2d) add to the growing hydrogen bonded water chain at  $\sim$ 75% RH, yielding ALP-MOF-1-7 $H_2O$ , and finally another seven water molecules, 08w-014w (013-019 in ALP-MOF-1-14H<sub>2</sub>O.cif), are observed upon saturation at ~100% RH (Figure 2e), giving ALP-MOF-1-14 $H_2O$ . The chemical formulas determined via SCXRD were confirmed using EA and TGA (Figure S3). Adsorption of these water molecules extends the W<sub>4</sub> chains and leads to gradual filling of the pores and formation of a complex water network, as observed from both the SCXRD data (Figure S10) and the optimized DFT structure refined from the periodic unit cell of ALP-MOF-1-14 $H_2O$  (Figure S22). In particular, at ~55% RH, a W<sub>6</sub> ring is formed in the middle of the pore (Figure 2c and Figure S10b), while at ~75% RH further growth of the water network in the pore leads to formation of a W<sub>12</sub> ring (Figure 2d and S10C). The increase in water loading leads to corresponding increases in calculated binding energies which reach average values per water molecule of 13.9 kcal/mol at ~55% RH and 14.7 kcal/mol at ~75% RH.

The number of 14 water molecules adsorbed at ~100% RH as determined by SCXRD is in excellent agreement with the number determined from the water adsorption isotherm. The water molecules form a (6,6,12)-connected hydrogen bonded water network within the pores (Fig. 3a, b, S10d), comprising 6-connected chair-shaped W<sub>12</sub> rings (Figure 3c,f), 12-connected W<sub>48</sub> clusters (Figure 3d,g), and 6connected W<sub>8</sub> cubes (Figure 3e,h). Six 08w and six 09w link together to form the W<sub>12</sub> ring, which sits in the large pore along the c crystallographic direction (Figure 3a,S11). The W<sub>48</sub> cluster is also centered in the large pore along c (Figure 3a,S12a,b) and has  $S_6$  point group symmetry. At its core it contains the W<sub>12</sub> ring identified in ALP-MOF-1-7H<sub>2</sub>O, formed by six 05w and six 07w linked by 05w···07w hydrogen bonds (Figure S12c). Branching from this core are six W6 chains consisting of 01w, 03w, 04w, 010w, 013w, 014w (Figure S12d). The W<sub>8</sub> cubes sit in the smaller pores (Figure S13) and consist of two 02w, two 06w, two 011w, and two 012w that are connected through 02w···06w, 02w···012w, 02w···012w, 06w···011w, 06w···012w, and 011w···012w hydrogen bonds. Additional insight into the water network formed at ~100% RH is provided in Figure S22 where its DFT optimized configuration in the MOF unit cell is provided. The calculated structure of the water network and of the framework atoms obey the R-3 hexagonal space group symmetry while the  $W_8$  cubes have local  $C_i$  symmetry. The calculated average adsorption energy per monomer mediated over all 252 water molecules in the unit cell at water saturation is calculated to be 16.5 kcal/mol.

metal ion exchange reaction yields transparent purple crystals (Figure 4a) that maintain the crystallinity of ALP-MOF-1, as evidenced by PXRD (Fig. S16). Based on its N<sub>2</sub> adsorp-

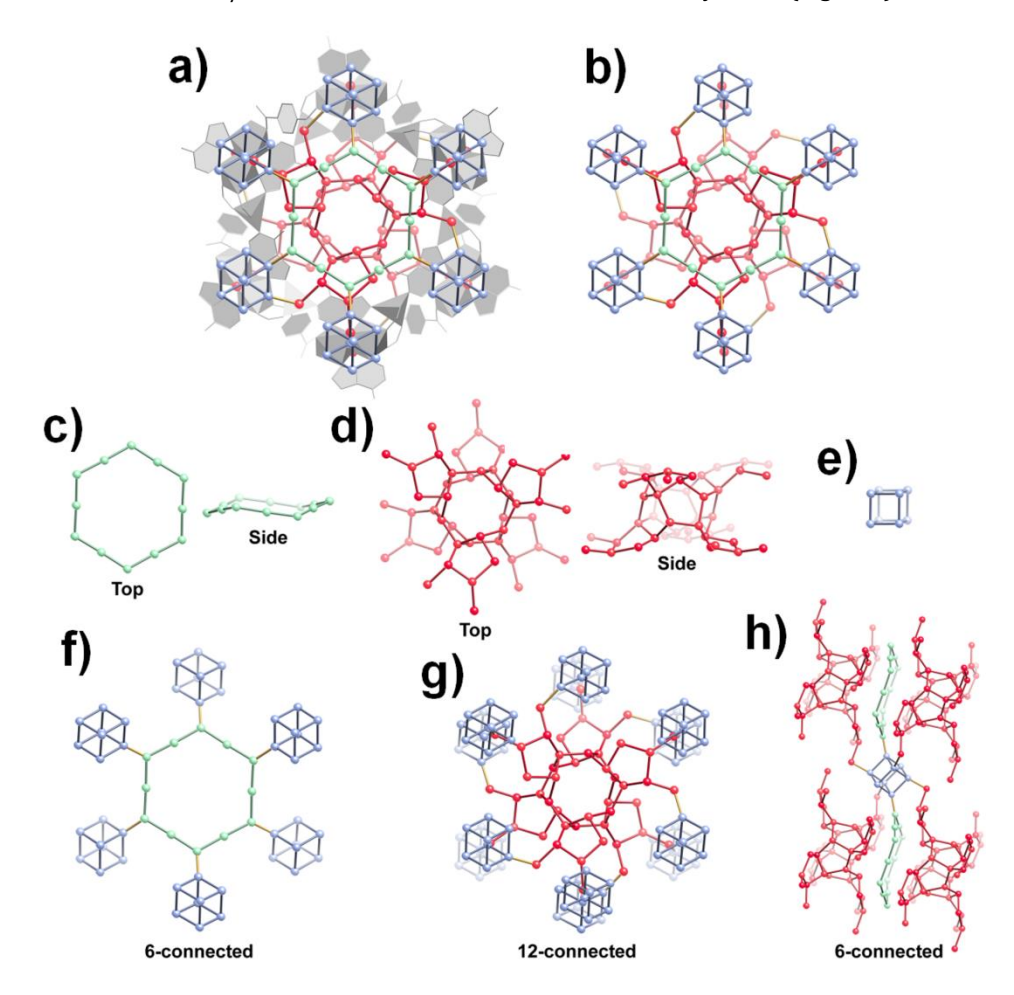


**Figure 3.** Single crystal structure of water network in ALP-MOF-1-14*H*<sub>2</sub>*O.* a) Extended water network consisting of interconnected water clusters (red, green, and blue). Spheres represent O atoms of individual adsorbed water molecules. Red, blue, and green lines between O atoms represent hydrogen bonds between water molecules within the clusters; gold lines between clusters represent hydrogen bonds between water molecules in neighboring clusters. MOF is shown in gray. b) Extended water network alone, without MOF. c) Top and side views of  $D_{3d}$  symmetric  $W_{12}$  cluster formed from alternating O8w and O9w linked by two O8w···O9w hydrogen bonds (2.857 Å and 2.870 Å). d) Top and side views of  $S_6$  symmetric  $W_{48}$  cluster formed from 01w, O3w, O4w, O5w, O7w, O10w, O13w, and O14w interlinked through six sets of ten different hydrogen bonds:  $O_{40} = O_{40} = O_{40}$ 

Adjusting Metal Content and Tuning Water Uptake Properties. The abrupt step in the water isotherm at ~23% RH corresponding to the adsorption of four water molecules suggests that tuning the identity of the metal sites could significantly affect the water uptake profile at low RH. Since Co(II) and Zn(II) have similar coordination preferences and because Co(II) is predicted to have a stronger interaction with water than Zn(II),<sup>39</sup> we targeted the isostructural Co(II) framework analogue via metal ion metathesis. Incubating single crystals of ALP-MOF-1-AS in a CH<sub>3</sub>CN solution of CoCl<sub>2</sub> at 50 °C for seven days yielded a cobalt-terephthalate-allopurinol MOF (ALP-MOF-2, Figure 4a). The

tion isotherm (77 K), ALP-MOF-2 is slightly less porous than ALP-MOF-1 (BET surface area  $\sim\!1860~m^2/g)$  (Figure 4b), which may be due to some unobservable defect formation during the metal metathesis process. The ALP-MOF-2 crystals were suitable for SCXRD analysis, which revealed definitively that ALP-MOF-2 and ALP-MOF-1 are isostructural (Table S2). ICP analysis revealed a 98.9:1.1 ratio of Co to Zn, indicating nearly quantitative metal exchange.

We expected Co(II) to coordinate more strongly with water molecules than Zn(II).<sup>39</sup> Indeed, the shorter Co(II)– $\mu_2$ -H<sub>2</sub>O bond lengths in ALP-MOF-2 compared to the Zn(II)– $\mu_2$ -H<sub>2</sub>O bond lengths in ALP-MOF-1-acetone (Figure 4c) suggests Co(II) has a stronger coordination affinity with water

than Zn(II). These stronger interactions are further supported by TGA data: complete removal of solvents, including water, from ALP-MOF-2 occurs at ~120 °C compared to ~75 °C for ALP-MOF-1-acetone (Figure S14a). Further, activated ALP-MOF-2 (ALP-MOF-2-A) formed by heating at 50 °C under vacuum for 12h readily adsorbs water from air, indicating strong water binding (Figure S14b,c). We anticipated that stronger water coordination in ALP-MOF-2-A would significantly affect water uptake at low RH based on our postulate that initial adsorption to the metal sites seeds water network formation in the MOF. Indeed, ALP-MOF-2-A exhibits gradual water uptake between zero and ~20% RH and clear absence of the abrupt concerted water adsorption step observed for ALP-MOF-1-A (Figure 4d). The lower total water capacity of ALP-MOF-2-A compared to ALP-MOF-1-A is consistent with its lower BET surface area (see above).

We again used SCXRD to track the water uptake, because ALP-MOF-2-A remains highly crystalline after exposure to water vapor at low RH (Figure S15). At ~4% RH, a single water molecule (O1w; O6 in ALP-MOF-2- $1H_2O$ .cif) terminally coordinates to each of the central Co(II) sites (ALP-MOF-2- $1H_2O$ ), forming a hydrogen bond with an O atom

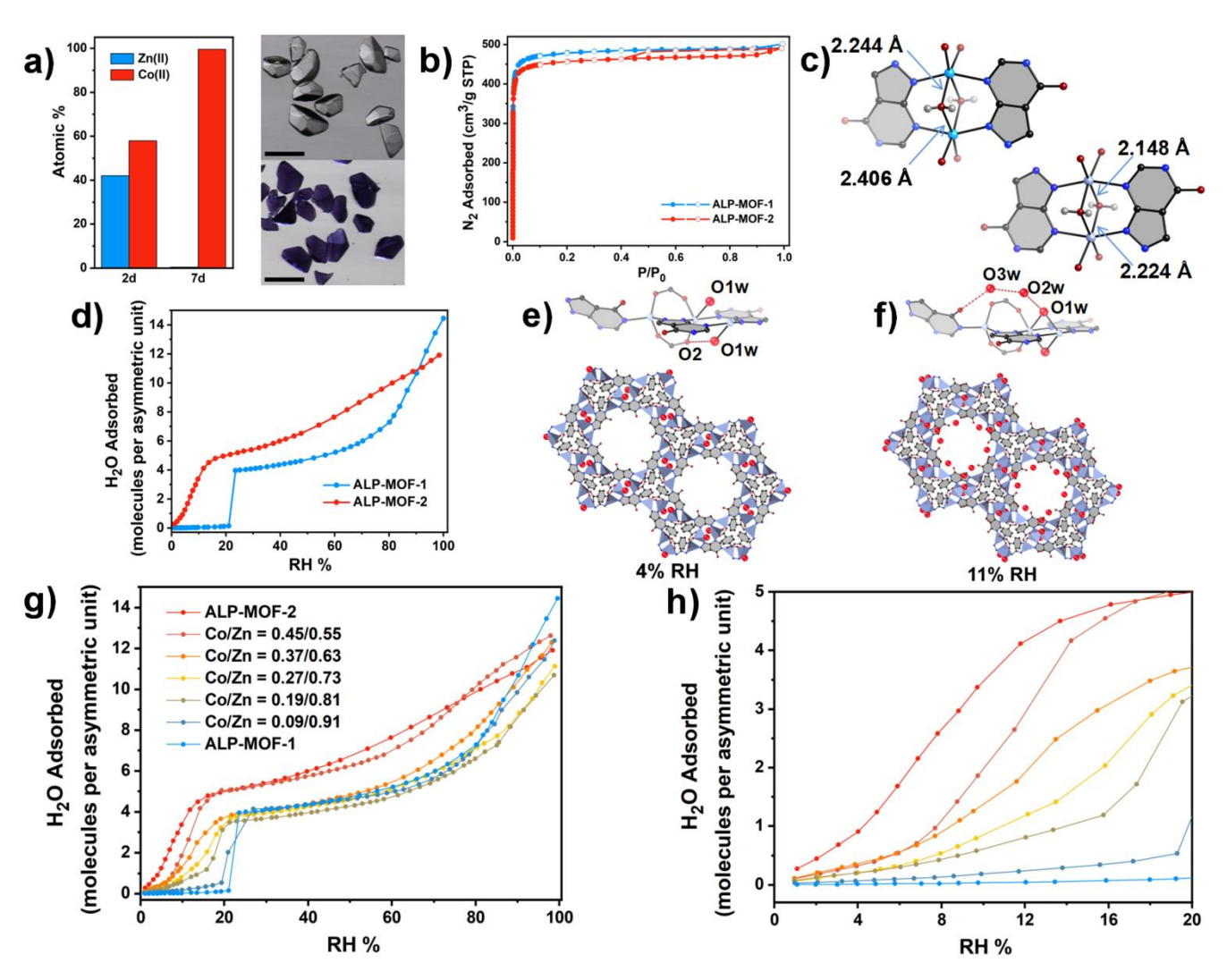


**Figure 4.** Comparison of ALP-MOF-1 and ALP-MOF-2 and Water Adsorption on ALP-MOF-2-*A* Mixed Metal Analogues. a) Bar graph showing Zn(II) and Co(II) content after 2d and 7d of soaking ALP-MOF-1-*AS* in Co(II) salt solution and optical microscope images of ALP-MOF-1-*acetone* (top) and ALP-MOF-2 (bottom); scale bar: 200 μm. b) Comparison of N<sub>2</sub> sorption isotherms (77 K) for ALP-MOF-1-*A* (blue) and ALP-MOF-2-*A* (red) (filled and empty circles are for adsorption and desorption, respectively). c) M(II) – $\mu$ 2-H<sub>2</sub>O bond lengths in ALP-MOF-1-*acetone* (top) and ALP-MOF-2 (bottom) (Zn, light blue; Co, light purple; C, black; N, dark blue; O, dark red; H, light gray). d) Comparison of water adsorption isotherms at 298 K for ALP-MOF-1-*A* (blue) and ALP-MOF-2-*A* (red). e,f) Two depictions of crystal structures: top, fragment around Co(II) cluster; bottom, view of channel along *c* crystallographic direction (Co, light purple spheres and polyhedra; C, black spheres; N, dark blue spheres; framework O, small dark red spheres; water O; large bright red spheres; H omitted for clarity). e) ALP-MOF-2-1*H*2O formed after exposure of ALP-MOF-2-A to ~4% RH (1 water molecule per asymmetric unit, O1w) (Co-O1w = 2.230 Å; O1w···O2 = 2.919 Å); dashed line between O2 and O1w indicates hydrogen bonding interaction. f) ALP-MOF-2-3*H*2O formed after exposure of ALP-MOF-2-A to ~11% RH (3 water molecules per asymmetric unit, O1w-O3w) (Co-O1w = 2.219 and 2.260 Å; O1w···O2w = 2.653 Å; O2w···O3w = 2.646 Å; O3w···O5 = 2.990 Å) ); dashed lines between O atoms indicate hydrogen bonding interactions. g) Water adsorption isotherms from 0-100% RH (298 K) as a function of Co/Zn ratio. h) Water adsorption isotherms from 0-20% RH (298 K) as a function of Co/Zn ratio.

ALP-MOF-2- $3H_2O$ ). At this loading, a  $W_3$  chain is formed, with an increase in the average water molecule calculated adsorption energy to 15.2 kcal/mol; the optimized configuration of this  $W_3$  chain was determined through refinement from the periodic unit cell of ALP-MOF-1- $4H_2O$  (Figure S23). Like ALP-MOF-1-A, ALP-MOF-2 shows reduced water uptake in a second water adsorption experiment (Figure S16a), yet it maintains its crystallinity after water adsorption (Figure S16b). Decomposition of these MOFs presumably occurs via gradual hydrolysis at the metal centers, leading to ligand displacement. Future studies will aim toward using

even more Lewis acidic metals to strengthen the M-ligand interactions.

The differences between the low RH regions of the water isotherms for ALP-MOF-1-A and ALP-MOF-2-A are striking: Co(II) enables gradual water uptake up to ~four-five molecules between 0 and ~23% RH while Zn(II) results in abrupt loading of ~four molecules at ~23% RH. We therefore reasoned that careful tuning of both the onset of water uptake and the slope of uptake from 0 to 20% RH should be possible by varying the Zn/Co ratio. Incomplete metathesis of Zn(II) with Co(II) was achieved by reducing the reaction time, allowing isolation of crystalline analogues (Figure S17) with the following Zn/Co ratios: 0.56:0.44, 0.45:0.55, 0.37:0.63, 0.27:0.73, 0.19:0.81, and 0.09:0.91, as determined by scanning electron microscopy-energy dispersive spectroscopy (SEM-EDS) on finely ground samples to ensure homogeneous sampling. Interestingly, the water isotherm for the 0.56:0.44 analogue closely resembles ALP-MOF-2-A in terms of shape and total water uptake (Figure S18), suggesting that the adsorption sites within these MOFs are very similar. Although we cannot determine the positions of Co and Zn from X-ray diffraction data, we currently postulate that the octahedral Zn(II) sites are preferentially replaced by Co(II) and the 0.56:0.44 analogue likely has ~2 central octahedral Co(II) and ~2 peripheral tetrahedral Zn(II). Our reasoning is based on the fact that the peripheral tetrahedral sites play no apparent role in influencing water uptake (i.e., they do not directly interact with adsorbed water) and replacing the two octahedral sites with Co(II) would essentially render the composition of the framework adsorption sites in ALP-MOF-2-A and the 0.56:0.44 analogue identical. As the ratio of Co/Zn transitions from 0.45:0.55 to 0:1, the water isotherms begin to gradually transition in terms of shape and capacity toward that observed for ALP-MOF-1-A (Figure 4g,h and S19), which would be expected if Zn(II) occupies a certain portion of the octahedral sites. These data clearly demonstrate that metal ion composition in MOFs can dramatically affect water adsorption properties and that precise adjustment of metal ion composition enables careful and deliberate tuning of these properties.

#### **CONCLUSIONS**

The fundamental experimental and computational studies presented herein illuminate MOF structural and chemical features that could be considered in the design and tuning of MOFs for water capture applications. They also highlight how multiple water anchoring sites, when placed in proximity, can be leveraged to realize unique water adsorption steps which could be useful for applications requiring energetically facile and rapid water adsorption/desorption cycles. Careful tuning of the chemical composition of these anchoring sites enables dramatic tuning of the water uptake properties.

## **EXPERIMENTAL METHODS**

### Syntheses of MOFs.

**Chemicals.** Zn(NO<sub>3</sub>)<sub>2</sub>·6H<sub>2</sub>O, CoCl<sub>2</sub>·6H<sub>2</sub>O, CH<sub>3</sub>COOK, NaBr, NaCl, CsF, LiCl, dimethylacetamide (DMA) and acetonitrile (CH<sub>3</sub>CN) were purchased from Sigma-Aldrich. Allopurinol (H<sub>2</sub>ALP) and terephthalic acid (H<sub>2</sub>BDC) were purchased

from TCI. Acetone was purchased from Fisher Scientific. NA-NOpure® (Thermo Scientific, > 18.2  $M\Omega\cdot cm$ ) water was used in the synthesis of the MOFs. All purchased chemicals were used without further purification.

**ALP-MOF-1-AS** (AS = as synthesized): A mixture of  $Zn(NO_3)_2 \cdot 6H_2O$  (297 mg, 1 mmol),  $H_2ALP$  (68 mg, 0.5 mmol), and  $H_2BDC$  (83 mg, 0.5 mmol) dissolved in DMA/ $H_2O$  (60 ml:10 mL) was heated at 100 °C for 12 h (Yield: ~80%). The block crystals were washed with fresh DMA (3×) and stored for further use. EA calcd (%) for  $Zn_2(\mu_2-H_2O)(ALP)(BDC) \cdot 2DMA, H_2O$  ( $C_{21}H_{28}N_6O_9Zn_2$ ): C, 39.45; H, 4.41; N, 13.15; Found: C, 39.23; H, 4.64; N, 13.19.

**ALP-MOF-1-***acetone*: ALP-MOF-1-*AS* was soaked in acetone for 5 days. During the process, acetone was refreshed 2 times per day. EA calcd (%) for  $Zn_2(\mu_2-H_2O)(ALP)(BDC)$ -acetone,2 $H_2O$  ( $C_{16}H_{18}N_4O_9Zn_2$ ): C, 35.51; H, 3.35; N, 10.35; Found: C, 36.01; H, 3.98; N, 10.56.

**ALP-MOF-1-***A* (A = activated): ALP-MOF-1-acetone was placed in a vacuum oven at room temperature for 24 h to give ALP-MOF-1-A. EA calcd (%) for  $Zn_2(ALP)(BDC)$  ( $C_{13}H_6N_4O_5Zn_2$ ): C, 36.39; H, 1.41; N, 13.06; Found: C, 36.25; H, 1.83; N, 13.22.

**ALP-MOF-1-***4H*<sub>2</sub>*O*: Exposing single crystals of ALP-MOF-1-*A* to a saturated CH<sub>3</sub>COOK solution (RH =  $\sim 23\%$ ) at room temperature overnight yields ALP-MOF-1-*4H*<sub>2</sub>*O*. EA calcd (%) for Zn<sub>2</sub>( $\mu_2$ -H<sub>2</sub>O)(ALP)(BDC)· $3H_2O$  (C<sub>13</sub>H<sub>14</sub>N<sub>4</sub>O<sub>9</sub>Zn<sub>2</sub>): C, 31.16; H, 2.82; N, 11.18; Found: C, 31.23; H, 3.09; N, 11.87. Note: A 20 ml vial with a syringe needle in the rubber cap was evacuated in vacuum oven at room temperature overnight prior to injecting 4 ml saturated CH<sub>3</sub>COOK solution. The vial with the saturated CH<sub>3</sub>COOK solution was allowed to stand overnight. Then, a 4 ml uncapped vial containing single crystals of ALP-MOF-1-*A* ( $\sim$ 15 mg) was rapidly transferred into the 20 ml vial and the 20 ml vial was then capped and allowed to stand overnight (Scheme 1 in the SI).

**ALP-MOF-1-5***H*<sub>2</sub>*O*: Exposing single crystals of ALP-MOF-1-*A* to a saturated NaBr solution (RH =  $\sim$ 55%) at 30 °C overnight yields ALP-MOF-1-5*H*<sub>2</sub>*O*. EA calcd (%) for Zn<sub>2</sub>( $\mu$ <sub>2</sub>-H<sub>2</sub>O)(ALP)(BDC)·4H<sub>2</sub>O (C<sub>13</sub>H<sub>16</sub>N<sub>4</sub>O<sub>10</sub>Zn<sub>2</sub>): C, 30.08; H, 3.11; N, 10.79; Found: C, 30.34; H, 3.58; N, 11.02.

**ALP-MOF-1-7** $H_2O$ : Exposing single crystals of ALP-MOF-1-A to a saturated NaCl solution (RH =  $\sim$ 75%) at room temperature overnight yields ALP-MOF-1- $7H_2O$ . EA calcd (%) for  $Zn_2(\mu_2-H_2O)$ (ALP)(BDC)· $6H_2O$  ( $C_{13}H_{20}N_4O_{12}Zn_2$ ): C, 28.13; H, 3.63; N, 10.09; Found: C, 28.61; H, 3.41; N, 10.15.

**ALP-MOF-1-14H**<sub>2</sub>**O**: Soaking single crystals of ALP-MOF-1-*A* ( $\sim$  15 mg) in 2 drops of water at room temperature for 2 h yields ALP-MOF-1-14H<sub>2</sub>O. EA calcd (%) for Zn<sub>2</sub>( $\mu$ <sub>2</sub>-H<sub>2</sub>O)(ALP)(BDC)·13H<sub>2</sub>O (C<sub>13</sub>H<sub>34</sub>N<sub>4</sub>O<sub>19</sub>Zn<sub>2</sub>): C, 22.92; H, 5.03; N, 8.22; Found: C, 23.08; H, 5.61; N, 8.02.

**ALP-MOF-2:** Incubating single crystals of ALP-MOF-1-AS ( $\sim$  50 mg) in a CH<sub>3</sub>CN solution of CoCl<sub>2</sub> (20 ml, 0.01 M) at 50 °C for 7 d yields ALP-MOF-2. The solution CoCl<sub>2</sub> solution was refreshed once per day. EA calcd (%) for Co<sub>2</sub>( $\mu_2$ -H<sub>2</sub>O)(ALP)(BDC)·3H<sub>2</sub>O,2CH<sub>3</sub>CN (C<sub>17</sub>H<sub>20</sub>N<sub>6</sub>O<sub>9</sub>Co<sub>2</sub>): C, 35.81; H, 3.53; N, 14.74; Found: C, 36.02; H, 3.21; N, 14.58. ICP for metal ion: Co (98.9%); Zn (1.1%). The as-synthesized sample was thoroughly washed with CH<sub>3</sub>CN for at least 5 d, and CH<sub>3</sub>CN was refreshed 3 times per day. Fully activated ALP-

MOF-2 (ALP-MOF-2-A) can be obtained by heating at 80 °C under vacuum for 12 h.

**ALP-MOF-2-1** $H_2O$ : Exposing single crystals of ALP-MOF-2-A to a saturated CsF solution (RH = ~4%) at room temperature overnight yields ALP-MOF-2- $1H_2O$  (Co<sub>2</sub>(H<sub>2</sub>O)(ALP)(BDC)). ALP-MOF-2- $1H_2O$  can rapidly adsorb water from air, so EA could not be performed.

**ALP-MOF-2-3H\_2O:** Exposing single crystals of ALP-MOF-2-A to a saturated LiCl solution (RH =  $\sim$ 11%) at room temperature overnight yields ALP-MOF-2- $3H_2O$  (Co<sub>2</sub>( $\mu_2$ - $H_2O$ )(ALP)(BDC)·2H<sub>2</sub>O). ALP-MOF-2- $3H_2O$  can rapidly adsorb water from air, so EA could not be performed.

**Mixed Co(II)/Zn(II) ALP-MOFs:** Incubating single crystals ALP-MOF-1-AS ( $\sim$  50 mg) in a CH<sub>3</sub>CN solution of CoCl<sub>2</sub> (20 ml, 0.01 M) at 50 °C can afford analogues with the following Co/Zn ratios (note: incubation time in parentheses): 0.56:0.44 ( $\sim$  48 h), 0.45:0.55 ( $\sim$  24 h), 0.37:0.63 ( $\sim$  12 h), 0.27:0.73 ( $\sim$  6 h), 0.19:0.81 ( $\sim$  3 h), and 0.09:0.91 ( $\sim$  0.5 h). The Co/Zn ratios were determined using SEM-EDS on thoroughly ground samples of the MOF crystals.

## ASSOCIATED CONTENT

**Supporting Information**. This material is available free of charge via the Internet at http://pubs.acs.org." Porosity studies, TGA, PXRD, SCXRD, ¹H NMR spectroscopy, FT-IR spectroscopy, EDS data, water sorption studies, and computation methods.

#### **Accession codes**

The X-ray crystallographic coordinates for structures reported in this article have been deposited at the Cambridge Crystallographic Data Centre (CCDC), under deposition nos. CCDC 2064996-2065002 for ALP-MOF-1-A, ALP-MOF-1-A, ALP-MOF-1-A, ALP-MOF-1-A, ALP-MOF-1-A, ALP-MOF-1-A, ALP-MOF-1-A, ALP-MOF-1-A, ALP-MOF-1-A, ALP-MOF-2-A, ALP-MOF-1-A, ALP-MOF-1-A,

## **AUTHOR INFORMATION**

## **Corresponding Author**

Yi Han - Department of Chemistry, University of Pittsburgh, Pittsburgh, Pennsylvania, United States.; orcid. org/0000-0003-0395-1111; Email: yih80@pitt.edu

Nathaniel L. Rosi - Department of Chemistry, University of Pittsburgh, Pittsburgh, Pennsylvania, United States.; Department of Chemical & Petroleum Engineering, University of Pittsburgh, Pittsburgh, Pennsylvania, United States.; orcid. org/0000-0001-8025-8906; Email: nrosi@pitt.edu

#### **Authors**

**Prasenjit Das** - Department of Chemistry, University of Pittsburgh, Pittsburgh, Pennsylvania, United States.

**Yiwen He** - Department of Chemistry, University of Pittsburgh, Pittsburgh, Pennsylvania, United States.

**Dan C. Sorescu** - U.S. Department of Energy, National Energy Technology Laboratory, Pittsburgh, Pennsylvania, United States; Department of Chemical & Petroleum Engineering, University of Pittsburgh, Pittsburgh, Pennsylvania, United States

**Kenneth D. Jordan** - Department of Chemistry, University of Pittsburgh, Pittsburgh, Pennsylvania, United States.; Department of Chemical & Petroleum Engineering, University of Pittsburgh, Pittsburgh, Pennsylvania, United States.

## **Author Contributions**

#Y.H. and P.D. contributed equally to this work.

#### Notes

The authors declare no competing financial interest.

## **ACKNOWLEDGMENT**

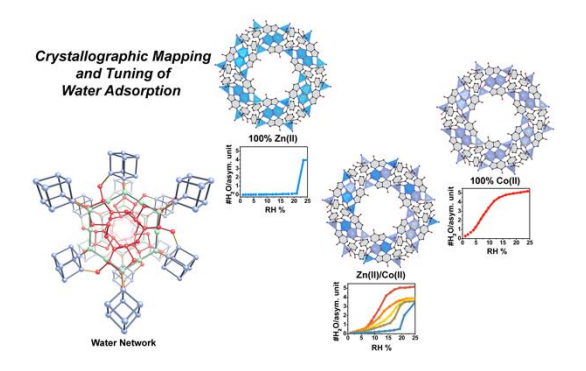
The authors acknowledge support from the University of Pittsburgh as well as partial support through an appointment to the Research Participation Program at the National Energy Technology Laboratory, U.S. Environmental Protection Agency, administered by the Oak Ridge Institute for Science and Education through an interagency agreement between the U.S. Department of Energy and EPA (NLR). This work was performed, in part, at the Nanoscale Fabrication and Characterization Facility, a laboratory of the Gertrude E. and John M. Petersen Institute of NanoScience and Engineering, housed at the University of Pittsburgh.

#### REFERENCES

- (1) Hiroyasu, F.; Cordova, K. E.; O'Keeffe, M.; Yaghi. O. M. The chemistry and applications of metal-organic frameworks. *Science*. **2013**, *341*, 1230444.
- (2) Kitagawa, S.; Kitaura, R.; Noro, S.-I. Functional porous coordination polymers. *Angew. Chem. Int. Ed.* **2004**, *43*, 2334–2375.
- (3) Murray, L. J.; Dincă, M.; Long, J. R. Hydrogen storage in metalorganic frameworks. *Chem. Soc. Rev.* **2009**, *38*, 1294–1314.
- (4) Li, J.-R.; Kuppler, R. J.; Zhou, H.-C. Selective gas adsorption and separation in metal-organic frameworks. *Chem. Soc. Rev.* **2009**, 38 1477–1504
- (5) Chen, B.; Xiang, S.; Qian. G. Metal-organic frameworks with functional pores for recognition of small molecules. *Acc. Chem. Res.* **2010**, *43*, 1115–1124.
- (6) Sumida, K.; Rogow, D. L.; Mason, J. A.; McDonald, T. M.; Bloch, E. D.; Herm, Z. R.; Bae, T. H.; Long, J. R. Carbon dioxide capture in metal-organic frameworks. *Chem. Rev.* **2012**, *112*, 724–781.
- (7) Liu, X.; Wang, X.; Kapteijn, F. Water and metal-organic frameworks: from interaction toward utilization. *Chem. Rev.* **2020**, *120*, 8303–8377
- (8) Rieth, A. J.; Yang, S.; Wang, E. N.; Dincă, M. Record atmospheric fresh water capture and heat transfer with a material operating at the water uptake reversibility limit. *ACS Cent. Sci.* **2017**, *3*, 668–672.
- (9) Kim, H.; Yang, S.; Rao, S. R.; Narayanan, S.; Kapustin, E. A.; Furukawa, H.; Umans, A. S.; Yaghi, O. M.; Wang, E. N. Water harvesting from air with metal-organic frameworks powered by natural sunlight. *Science*. **2017**, *356*, 430–434.
- (10) Xu, W.; Yaghi, O. M. Metal-organic frameworks for water harvesting from air, anywhere, anytime. *ACS Cent. Sci.* **2020**, *6*, 1348–1354.
- (11) Hanikel, N.; Prévot, M. S.; Yaghi, O. M. MOF water harvesters. *Nat. Nanotechnol.* **2020**, *15*, 348–355.
- (12) Cadiau, A., Belmabkhout, Y., Adil, K., Bhatt, P. M., Pillai, R. S., Shkurenko, A., Martineau-Corcos, C., Maurin, G., & Eddaoudi, M. Hydrolytically stable fluorinated metal-organic frameworks for energy-efficient dehydration. *Science*. **2017**, *356*, 731–735.
- (13) AbdulHalim, R. G.; Bhatt, P. M.; Belmabkhout, Y.; Shkurenko, A.; Adil, K.; Barbour, L. J.; Eddaoudi, M. A Fine-tuned metal-organic

- framework for autonomous indoor moisture control. *J. Am. Chem. Soc.* **2017**, *139*, 10715–10722.
- (14) Wang, S.; Lee, J. S.; Wahiduzzaman, M.; Park, J.; Muschi, M.; Martineau-Corcos, C.; Tissot, A.; Cho, K. H.; Marrot, J.; Shepard, W.; Maurin, G.; Chang, J.-S.; Serre, C. A robust large-pore zirconium carboxylate metal-organic framework for energy-efficient watersorption-driven refrigeration. *Nat. Energy.* **2018**, *3*, 985–993.
- (15) Rowsell, J. L. C.; Spencer, E. C.; Eckert, J.; Howard, ; Yaghi, O. M. Gas adsorption sites in a large-pore metal-organic framework. *Science.* **2005**, *309*, 1350–1354.
- (16) Yan, Y.; Telepeni, I.; Yang, S.; Lin, X.; Kockelmann, W.; Dailly, A.; Blake, A. J.; Lewis, W.; Walker, G. S.; Allan, D. R.; Barnett, S. A.; Champness, N. R.; Schröder, M. Metal-organic polyhedral frameworks: high  $H_2$  adsorption capacities and neutron powder diffraction studies. *J. Am. Chem. Soc.* **2010**, *132*, 4092–4094.
- (17) Vaidhyanathan, R.; Iremonger, S. S.; Shimizu, G. K. H.; Boyd, P. G.; Alavi, S.; Woo, T. K. Direct observation and quantification of CO2 binding within an amine-functionalized nanoporous solid. *Science.* **2010**, *330*, 650–653.
- (18) Bloch, W. M.; Burgun, A.; Coghlan, C. J.; Lee, R.; Coote, M. L.; Doonan, C. J.; Sumby, C. J. Capturing snapshots of post-synthetic metallation chemistry in metal-organic frameworks. *Nat. Chem.* **2014**, *6*, 906–912.
- (19) Banerjee, D.; Simon, C. M.; Plonka, A. M.; Motkuri, R. K.; Liu, J.; Chen, X.; Smit, B.; Parise, J. B.; Haranczyk, M.; Thallapally, P. K. Metal-organic framework with optimally selective xenon adsorption and separation. *Nat. Commun.* **2016**, *7*, 11831.
- (20) Huang, R.-W.; Wei, Y.-S.; Dong, X.-Y.; Wu, X.-H.; Du,C.-X.; Zang, S.-Q.; Mak, T. C. W. Hypersensitive dual-function luminescence switching of a silver-chalcogenolate cluster-based metal-organic framework. *Nat. Chem.* **2017**, *9*, 689–697.
- (21) Liao, P.-Q.; Huang, N.-Y.; Zhang, W.-X.; Zhang, J.-P.; Chen, X.-M. Controlling guest conformation for efficient purification of butadiene. *Science*. 2017, 356, 1193–1196.
- (22) Smith, G. L.; Eyley, J. E.; Han, X.; Zhang, X.,; Li, J.; Jacques, N. M.; Godfrey, H. G. W.; Argent, S. P.; McCormick McPherson, L. J.; Teat, S. J.; Cheng, Y.; Frogley, M. D.; Cinque, G.; Day, S. J.; Tang, C. C.; Easun, T. L.; Rudić, S.; Ramirez-Cuesta, A. J.; Yang, S.; Schröder, M. Reversible coordinative binding and separation of sulfur dioxide in a robust metal-organic framework with open copper sites. *Nat. Mater.* **2019**, *18*, 1358–1365.
- (23) Zeng, H.; Xie, M.; Wang, T.; Wei, R.-J.; Xie, X.-J.; Zhao, Y.; Lu, W.; Li, D. Orthogonal-array dynamic molecular sieving of propylene/propane mixtures. *Nature*. 2021, 595, 542–548.
- (24) Furukawa, H.; Gándara, F.; Zhang, Y.-B.; Jiang, J.; Queen, W. L.; Hudson, M. R.; Yaghi, O. M. Water adsorption in porous metalorganic frameworks and related materials. *J. Am. Chem. Soc.* **2014**, *136*, 4369–4381.
- (25) Abtab, S. M. T.; Alezi, D.; Bhatt, P. M.; Shkurenko, A.; Belmabkhout, Y.; Aggarwal, H.; Weselinski, Ł. J.; Alsadun, N.; Samin, U.; Hedhili, M. N.; Eddaoudi, M. Reticular chemistry in action: A hydrolytically stable MOF capturing twice its weight in adsorbed water. *Chem.* **2018**, *4*, 94–105.

- (26) Rieth, A. J.; Hunter, K. M.; Dincă, M.,; Paesani, F. Hydrogen bonding structure of confined water templated by a metal-organic framework with open metal sites. *Nat. Commun.* **2019**, *10*, 4771.
- (27) Burtch, N. C.; Walton, I. M.; Hungerford, J. T.; Morelock, C. R.; Jiao, Y.; Heinen, J.; Chen, Y.-S.; Yakovenko, A. A.; Xu, W.; Walton, K. S. In situ visualization of loading-dependent water effects in a stable metal–organic framework. *Nat. Chem.* **2020**, *12*, 186–192.
- (28) Ichii, T.; Arikawa, T.; Omoto, K.; Hosono, N.; Sato, H.; Kitagawa, S.,; Tanaka, K. Observation of an exotic state of water in the hydrophilic nanospace of porous coordination polymers. *Communications Chemistry.* **2020**, *3*, 16.
- (29) Hanikel, N.; Pei, X.; Chheda, S.; Lyu, H.; Jeong, W. S.; Sauer, J.; Gagliardi, L.; Yaghi, O. M. Evolution of water structures in metalorganic frameworks for improved atmospheric water harvesting. *Science.* **2021**, *374*, 454–459.
- (30) Lin, R. B.; Xiang, S;, Zhou, W.; Chen, B. Microporous metalorganic framework materials for gas separation. *Chem.* **2020**, *6*, 337–363.
- (31) An, J.; Geib, S. J.; Rosi, N. L. Cation-triggered drug release from a porous zinc-adeninate metal-organic framework. *J. Am. Chem. Soc.* **2009**, *131*, 8376–8377.
- (32) An, J.; Farha, O. K.; Hupp, J. T.; Pohl, E.; Yeh, J. I.; Rosi, N. L. Metal-adeninate vertices for the construction of an exceptionally porous metal-organic framework. *Nat. Commun.* **2012**, *3*, 604.
- (33) Li, T.; Kozlowski, M. T.; Doud, E. A.; Blakely, M. N.; Rosi, N. L. J. Am. Chem. Soc. **2013**, *135*, 10011–10013.
- (34) Chen, L.; Ye, J.-W.; Wang, H.-P.; Pan, M.; Yin, S.-Y.; Wei, Z.-W.; Zhang, L.-Y.; Wu, K.; Fan, Y.-N.; Su, C.-Y. Ultrafast water sensing and thermal imaging by a metal–organic framework with switchable luminescence. *Nat. Commun.* **2017**, *8*, 15985.
- (35) Sigala, P. A.; Ruben, E. A.; Liu, C. W.; Piccoli, P. M. B.; Hohenstein, E. G.; Martínez, T. J.; Schultz, A. J.; Herschlag, D. Determination of hydrogen bond structure in water versus aprotic environments to test the relationship between length and stability. *J. Am. Chem. Soc.* **2015**, *137*, 5730–5740.
- (36) VandeVondele, J.; Krack, M.; Mohamed, F.; Parrinello, M.; Chassaing, T.; Hutter, J. Quickstep: Fast and accurate density functional calculations using a mixed gaussian and plane waves approach. *Comput. Phys. Commun.* **2005**, *167*, 103-128.
- (37) Perdew, J. P.; Burke, K.; Ernzerhof, M. Generalized gradient approximation made simple. *Phys. Rev. Lett.* **1996**, *77*, 3865-3868.
- (38) Grimme, S.; Antony, J.; Ehrlich, S.; Krieg, H. A consistent and accurate ab initio parametrization of density functional dispersion correction (DFT-D) for the 94 elements H-Pu. *J. Chem. Phys.* **2010**, *132*, 154104-154119.
- (39) Lee, K.; Howe, J. D.; Lin, L.-C.; Smit, B.; Neaton, J. B. Small-molecule adsorption in open-site metal-organic frameworks: a systematic density functional theory study for rational design. *Chem. Mater.* **2015**, *27*, 668–678.



For Table of Contents Only